



Research Article

## Parameter optimization of coriolis mass flow meter in laminar flow regime using Doe-Taguchi method

Vikram KOLHE<sup>1,\*</sup>, Suyash PAWAR<sup>2</sup>, Vishal CHAUDHARI<sup>3</sup>, Ravindra EDLABADKAR<sup>4</sup>, Sandipkumar SONAWANE<sup>5</sup>

<sup>1</sup>Department of Mechanical Engineering, Late G.N. Sapkal College of Engineering, Nashik, Maharashtra, 422212, India

<sup>2</sup>Department of Mechanical Engineering, MVPS's KBT College of Engineering, Nashik, Maharashtra, 422002, India

<sup>3</sup>Department of Mechanical Engineering, Cusrow Wadia Institute of Technology, Pune, Maharashtra, 411001, India

<sup>4</sup>Department of Mechanical Engineering, Pune Vidyarthi Griha's College of Engineering and Technology, Pune, Maharashtra, 422004, India

<sup>5</sup>Department of Mechanical Engineering, MVPS's KBT College of Engineering, Nashik, Maharashtra, 422002, India

### ARTICLE INFO

#### Article history

Received: 28 December 2022

Revised: 07 June 2023

Accepted: 16 June 2023

#### Keywords:

Coriolis Mass Flow Meter; Error Analysis; Analysis of Variance; Taguchi Approach; Laminar Flow; Tube Configuration

### ABSTRACT

The paper outlines the progression of a mathematical model using the Taguchi approach to analyze the performance of a Coriolis mass flow meter (CMFM). The sensor position, excitation frequency, and flow rate parameters were optimized using the Taguchi method for the meter's maximum time-lag output. An orthogonal array of experiments was designed, and the time lag results were obtained for two tube configurations (viz. Omega and Diamond) and parameter levels. The obtained data was analyzed using analysis of variance (ANOVA) to understand the relationship between the variables and the time lag. The results showed that the Omega tube configuration exhibited a lower percentage error compared to the Diamond tube configuration. Additionally, an increase in flow rate led to a decrease in the error. The regression models fitted the experimental data well, with high  $R^2$  values indicating a good fit. The ANOVA showed the factors' importance in affecting the time lag and the levels of interaction between the best individual parameters for maximizing the outcome. The most important factors affecting the Omega and Diamond tube configurations' maximum performance have been identified as the flow rate and sensor position, respectively. This study offers a systematic method for optimizing sensor parameters and provides light on how CMFMs behave in laminar flow. The experimental setup and mathematical model also serve as a basis for future research and advancements in CMFM design and functionality.

**Cite this article as:** Kolhe V, Pawar S, Chaudhari V, Edlabadkar R, Sonawane S. Parameter optimization of coriolis mass flow meter in laminar flow regime using Doe-Taguchi method. J Ther Eng 2023;9(4):1026–1040.

#### \*Corresponding author.

\*E-mail address: [kolhe.vikram@gmail.com](mailto:kolhe.vikram@gmail.com)

This paper was recommended for publication in revised form by Editor in Chief Ahmet Selim Dalkılıç



## INTRODUCTION

Due to its high accuracy, good repeatability, dependability, and consistent performance independent of changing fluid parameters, the Coriolis Mass Flow Meter (CMFM) is frequently employed as a mass flow measurement device. It has attracted market interest as a direct mass flow measurement instrument for a variety of industrial and natural fluid flow applications. Most applications involve turbulent flows, although some viscous fluids, like oils, can still display laminar flow even at high flow rates. Accurate metering is crucial in these circumstances since flow rate values may be much lower. The development of the CMFM includes continual efforts to maximize the Coriolis force and improve meter sensitivity. It is well known that the meter's performance varies depending on the tube configuration, sensor position, vibration frequency, and other factors. It has been noted that in the laminar flow area, the secondary shear force predominates over the Coriolis force, which reduces meter performance [1]. Gupta et al. [2] predicted the optimum sensor location through experimentation for certain shapes of sensor tubes for maximum meter reading. Sharma et al. [3] presented the error analysis for U-shaped sensor tubes for three L/D ratios (ratio of length of the tube to distance between two limbs of the U tube). They have further determined the optimum levels of parameters, including frequency and sensor position, for triangular copper tubes using response surface modelling [4]. Patil et al. [5] presented the influence of various meter parameters on the performance of the meter using the adaptive neuro-fuzzy inference system (ANFIS) and commented about its applicability as an alternative to the physical model. The phase shift and mass flow rate were modelled by the adaptive neuro-fuzzy inference system (ANFIS) to predict the effect of various design parameters and tube materials [6] on the performance of copper omega type CMFM. The authors reported that ANFIS can be effectively utilized to predict the input-output relationship with available experimental data. Patil et al. also used a neural network approach to predict the performance of the omega tube type Coriolis mass flow sensor [7, 8] and noted a good agreement level between predicted and experimental results. Furthermore, they mentioned the extensive capability of this model to handle any combination of factors with accuracy and reliability. Kolhe et al. [9] analyzed four distinct tube configurations for various parameters using both numerical and experimental methods, and he reported the ideal set of parameters for the best meter performance in the laminar area.

Tube shape significantly affects the performance of the CMFM, particularly measurement sensitivity, which should be high to reduce the effect of sensor noise on the measured mass flow. The drop in pressure between the inlet and outlet of the tube should be low, and the envelope of the tube should be small. These issues can be considered objectives or constraints for optimizing tube shape, depending on

their relative importance. The last issue is directly related to the tube shape, while the other two depend on the tube shape indirectly [11–12]. Based on the Euler beam model, a theoretical investigation of the fluid-solid interactions of the U-tube in a Coriolis mass flow meter using liquid hydrogen as the working fluid was presented. For comparison, the results for water and liquid nitrogen were reported. The results aid in the design optimization of a meter by analysing the effects of geometric parameters on the time lag for the three fluids. Investigations were done into how the sensor position, tube structure, and fluid flow velocity affected the vibration characteristics [13]. Ghalme et al. [14] used the Taguchi technique to optimize the machining parameters in order to reduce the surface roughness when milling glass fiber reinforced plastic (GFRP), and they identified speed as the main influencing factor. A further attempt was undertaken by Ghalme et al. [15] to examine the wear loss behavior of a Si<sub>3</sub>N<sub>4</sub>-hBN composite and assess the impact of adding hBN to Si<sub>3</sub>N<sub>4</sub> in order to reduce wear loss. The planning and analysis of experiments are done using the DoE-Taguchi technique. It has been discovered that wear performance depends on the load and hBN percentage. To study the wear behavior of silicon nitride (Si<sub>3</sub>N<sub>4</sub>)-hexagonal boron nitride (hBN), Ghalme et al. [16] used the integrated Taguchi-simulated annealing (SA) method. For the purpose of minimizing the wear rate in Si<sub>3</sub>N<sub>4</sub> against a steel counter face, the Taguchi analysis and SA optimization's best values for load and volume of hBN are reported.

Khan et al. [17] conducted a theoretical investigation of the actions of a bio-convective Maxwell nanofluid over an exponentially stretched sheet. The authors looked into how bio convection affected the system using equations for fluid flow and heat transfer. The findings showed that the presence of bio convection had a significant impact on fluid flow and heat transmission. By examining how bio convection influences micropolar fluid flow and heat transmission, Nadeem et al. [18] addressed the mathematical analysis of bio-convective micropolar nanofluids. According to the authors, bio convection sped up the rate of heat transfer while slowing fluid flow. Khan et al. [19] examined the temperature-dependent transport characteristics of micropolar fluid flow. The authors looked at the impact of temperature-dependent viscosity and thermal conductivity on fluid flow and heat transmission. The results showed that increasing the thermal conductivity and temperature-dependent viscosity increased the fluid flow rate and heat transfer rate. Using the Cattaneo-Christov heat flux model, Ahmad et al. [20] examined the stagnation point flow of micropolar nanofluids towards a nonlinear stretching surface with slip effects. The authors looked at how different parameters affected heat transfer and fluid flow, and the results showed that the slip effect had a big impact on the system. Ahmad et al. [21] studied the transmission of heat and mass in a Maxwell fluid with double stratification. The scientists looked at how fluid flow and heat transfer behaved in various situations and found that

double stratification accelerated both heat transfer and fluid flow. Khan et al. [22] investigated the transient Maxwell nanofluid flow across a contracting surface. The diminishing surface had a major impact on the system, according to the authors' investigations into the fluid flow and heat transfer behavior under various conditions. The MHD flow of a Maxwell fluid with thermophoretic and stratification effects in the direction of a stretching sheet was studied by Khan et al. [23]. In the analysis of heat and mass transmission, the Cattaneo-Christov theory and variable thermal conductivity were presented. It has been discovered that thermal and concentration stratification parameters minimize temperature and concentration distribution.

Khan et al. [24] investigated the theoretical treatment of radiative Oldroyd-B nanofluids with microorganisms moving across an exponentially stretching sheet. The authors looked at how various parameters affected fluid flow and heat transmission, and they found that radiative heat transfer had a big effect on the system. A comparison analysis of a rotating Maxwell nanofluid flow with linear and exponential stretching sheets with double stratification was provided by Nadeem et al. [25]. The authors looked at how fluid flow and heat transfer behaved under various circumstances and found that double stratification with an exponential stretching sheet accelerated both heat transfer and fluid flow.

Computational fluid dynamics (CFD) is used by Haider et al. [26] to analyse heat exchanger systems. The finite volume technique (FVM) is used in this work to analyse fluid resistance and heat transfer in a rectangular duct with obstructions. The accuracy of the model is confirmed by comparing CFD findings with experimental data, which also indicates the considerable impact of temperature, fluid flow rate, and velocity distribution on pressure and temperature inside the duct. Haider et al. [27] developed a computer model to investigate heat transmission in a square cavity. The study employs a novel finite volume (FV) method with adaptive upwind convection to accurately analyse the two-dimensional steady flow. The research focuses on understanding the consequences of temperature differences and convection within the cavity, driven by the industrial sector's interest in natural convection and its impact on heat transfer rates. The mass balance, momentum balance, and energy balance equations are examined in the context of a square cavity. Raza et al. [28] synthesised and characterised cobalt oxide (Co<sub>3</sub>O<sub>4</sub>) nanoparticles using the hydrothermal method. The study observed that higher synthesis temperatures resulted in larger particle sizes ranging from 13.62 nm to 17.81 nm. The nanoparticles exhibited a non-uniform distribution and sharp grain boundaries. Electrical characterization indicated semiconducting behaviour, with decreasing resistivity as temperature increased. The Co<sub>3</sub>O<sub>4</sub> nanoparticles showed potential for detecting hydrogen peroxide (H<sub>2</sub>O<sub>2</sub>). Nadeem et al. [29] performed numerical simulations to study fluid flow and convection in a two-dimensional rectangular cavity

with rotating obstacles. The effects of Reynolds and Prandtl numbers on heat transfer characteristics were investigated. The simulations revealed the importance of Reynolds and Prandtl numbers in determining velocity, pressure, vorticity, and temperature distributions within the system. Asghar et al. [30] investigated the efficiency of the perturbation method in solving nonlinear partial differential equations (PDEs). The study applied the perturbation technique to solve the zeroth-order Airy equation and a first-order non-homogeneous differential equation related to the modified Korteweg-de Vries (KdV) equation. The results demonstrate the potential of the perturbation method for solving nonlinear equations in physics and applied mathematics. By employing a stenosed elliptic conduit and the well-known Finite Volume Method (FVM), Haider et al. [31] studied the mechanical properties of a Rabinowitsch fluid model. The fluid flow through the ducts is investigated using a CFD model based on the FVM and experimental data from a flow cell. In this investigation, the pressure, velocity, and temperature fields of a fluid flowing through a stenosed duct are the main topics of interest. Rahman et al. [32] conducted a computational analysis of a Rabinowitsch fluid model in a stenosed elliptic conduit using computational fluid dynamics (CFD) and the finite volume method (FVM). The study validated the model by comparing CFD results with experimental data and analysing the pressure, velocity, and temperature fields in the stenosed duct. Haider et al. [33] proposed a variational iterative method with Laplace transformation to solve nonlinear partial differential equations (PDEs) and ordinary differential equations (ODEs). They applied this method to solve the highly nonlinear evolution of a simple pendulum and compared its results to those of other approaches. The variation iterative method showed accuracy in solving nonlinear oscillators with various time and boundary conditions. Zahid et al. [34] investigated quaternion differential equations (QDEs), a distinct type of differential equation that differs from ordinary differential equations. The study focused on obtaining exponential matrices for QDEs, which are crucial for solving quaternion-valued differential equations. The research explored fundamental quaternion concepts and employed the right eigenvalue method to develop a fundamental matrix, enabling the construction of exponential matrices necessary for QDE solutions. Haider et al. [35] proposed the Jacobi elliptic function expansion method as a versatile approach for solving nonlinear wave equations. It offers a broader range of solutions, including periodic, solitary, and shock wave solutions. This method enhances the analysis and solution of nonlinear wave equations.

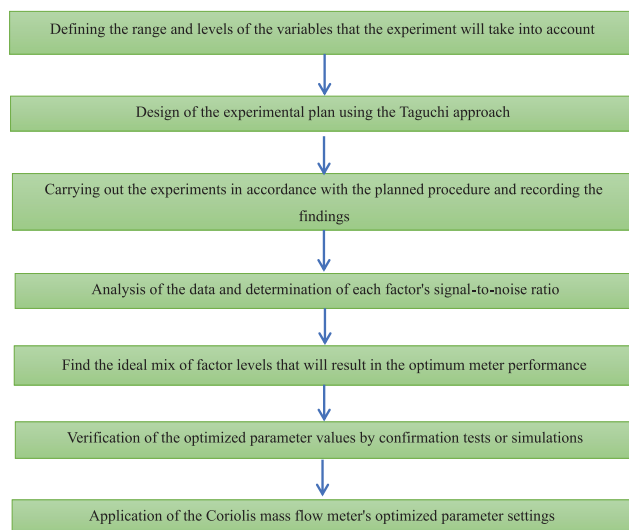
The originality of this study lies in the optimization of the Coriolis mass flow meter settings to increase measurement sensitivity in the laminar flow region, where the meter has a tendency to under read mass flow rate. The study aims to improve meter performance, especially in the laminar flow regime, where accurate metering is crucial since the secondary shear force predominates over the

Coriolis force and reduces meter performance. In order to determine the optimal set of parameters for the meter’s peak performance, the work employs a variance analysis for the parameters for the two different tube configurations, Omega and Diamond.

**Development of the Experimental Setup to Measure the Time Lag**

A systematic experimental setup was designed and developed to investigate the performance of Coriolis mass flow meters (CMFM) with various tube configurations in the laminar flow regime. The experiments were carried out using water as the working fluid, and the setup was designed to be flexible enough to accommodate different tube configurations and predict the effect of various working parameters on the performance of the sensor tube. The flow was controlled by two ball valves, while an exciter was used to vibrate the tube at a specific frequency and amplitude. The flow rate was measured using the conventional method of collecting the fluid in a container for a specific time, and the time lag was measured using an indigenously developed time lag measurement unit comprising an Arduino board.

**METHODOLOGY**



The movement of the sensor tube on the inlet and exit sides of the flow is detected using two optical IR (infrared) sensors. In essence, the sensor is a photo-interrupter module with an IR transmitter on one side and a receiver on the other. Tube configurations are given oscillatory motion at operating frequency using an electromagnetic vibration exciter with a power oscillator. A power amplifier can change the vibration’s amplitude and frequency to the desired value. A mild steel bolt is used as a stinger to transmit excitation to the tube arrangement. The experimentation was performed on two tube shapes (Omega and Diamond) for three sensor positions (SP1, SP2, and SP3)

and three frequencies of each tube (F1, F2, and F3). Here, F2 is the natural frequency, while F1 and F3 denote -10% and +10% of the natural frequency, respectively. The setup comprised various components and instruments, as shown in Fig. 1, and the experimental procedure was conducted in a meticulous manner to ensure the reliability and accuracy of the results, as mentioned below.

The guarantee of a zero reading at the beginning of each reading cycle ensured the fidelity of the sensors in a no-flow scenario. A thermometer was used to record the water’s temperature. An outlet ball valve opening was used to regulate the flow so that it was set at a rate within a pre-determined range. To assure accuracy in measurement, the discharge was measured at the start and end of the reading cycle. In accordance with the numerical simulation’s chosen tube configuration centerline, the sensor site was modified. The natural frequency was chosen for the vibration exciter in the numerical simulation. Throughout the experiment, the tube vibration’s amplitude is held constant at 6 mm from peak to peak.

The time lag ( $\Delta t$ ) measurements on the time lag measuring device were recorded for duration of 120 seconds, and then the average was calculated. This is performed for a variety of reasons under the regime of laminar flow. To reduce measurement error, the time lag ( $\Delta t$ ) readings for specific flows were repeated. The uncertainties associated with the input parameters, such as the water temperature, discharge measurements, and time lag measurements, were estimated. Volume measurement during the experiment showed a 5% level of inaccuracy. Additionally, a time count error of less than 1% was noted.

The study of fluid-structure interaction (FSI) and various experiments conducted in this field [9] have determined the ideal levels of meter parameters required to achieve maximum phase shift of the sensor tube in the laminar flow region. These investigations have resulted in optimised combinations of different meter parameters that can be used to predict the performance of different tube configurations. However, in order to ensure the accuracy of the obtained results, it is necessary to perform an error analysis. Additionally, it is essential to compute a flow correction factor (FCF) to ensure that the results are in line with the expected level of accuracy. In this regard, an analytical approach [3] has been used to determine the mass flow rate using the following expression:

$$\dot{m} = \frac{K_s \Delta t}{8d_1^2} \tag{1}$$

In the above expression, the torsional stiffness  $K_s$  is derived by analysing the motion of sensor tube using Castigliano’s second theorem [3] and is expressed using relation.

$$K_s = \frac{4EI d_1^2}{H^3} \left[ \frac{1 + \frac{3n_1}{4k} + 8n_1^3}{1 + \frac{3n_1}{4k}} \right] \tag{2}$$

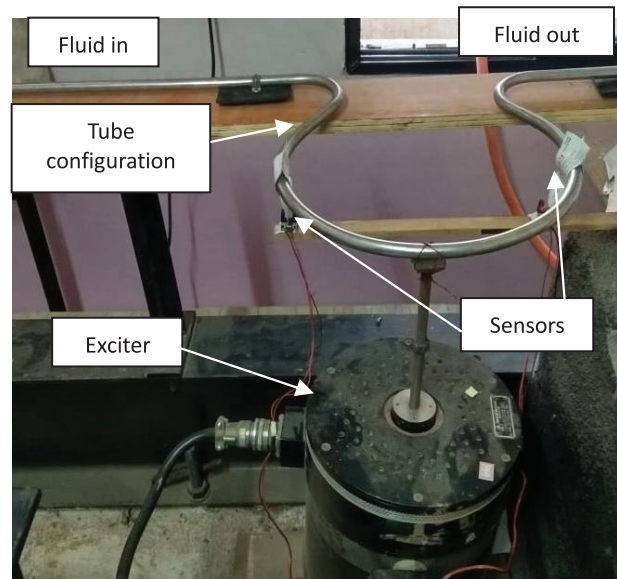
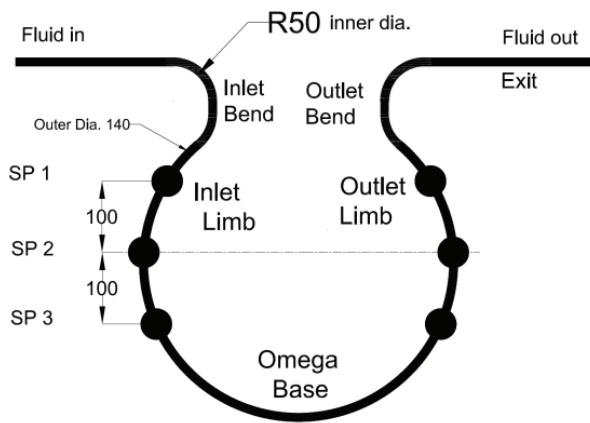
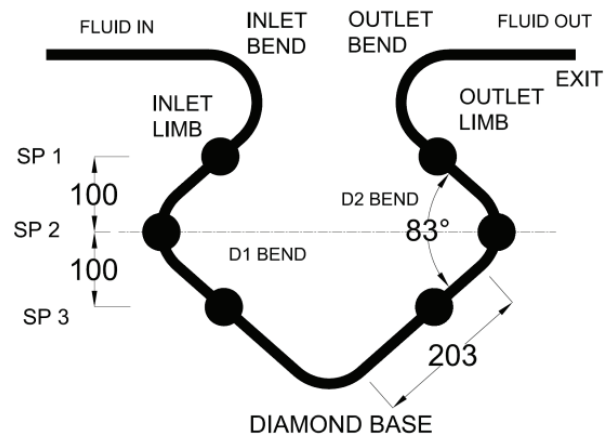


Figure 1. Experimental setup.



(a) Omega tube configuration



(b) Diamond tube configuration

Figure 2. Sensor positions for selected tube configurations.

The geometric parameters of selected tube configurations, viz. Omega and Diamond shapes, as shown in Fig. 2 and made of SS 304, have been listed in Table 1.

Table 1. Geometric parameters of selected tube configurations

Tube Configuration	H (m)	2d1 (m)	n1= H /d1
Omega	0.3	0.27	2.22
Diamond	0.4	0.45	1.78

The material properties of SS 304 and other parameters were taken as  $E = 210$  GPa, Poisson's ratio  $k = 0.275$ , internal diameter of the tube  $D_i = 12$  mm, tube thickness = 1.3 mm, flow range  $Re = 600$  to 1800, and amplitude of vibration = 6 mm peak to peak.

Similarly, the actual mass flow rate as measured during the experimentation is defined as [10],

$$\dot{m} = K \Delta t \tag{3}$$

Hence, the  $K_s$  and  $K$  can be related by a correction factor 'C' as [10],

$$K = C \frac{K_s}{8d_1^2} \tag{4}$$

The values of  $K_s$  for the selected tube configurations are calculated using expression (2) and corresponding values of ‘C’ have been summarized in Table 2.

**Table 2.** Torsional stiffness and correction factor of selected tube configurations

Tube Configuration	$K_s$ (Nm/rad)	Flow Correction Factor ‘C’
Omega	4665.94	0.0164
Diamond	3535.22	0.996

Furthermore, the overall uncertainty in the measurement of  $K_s$ , assuming the uncertainties in the parameters such as,  $E = 210 \text{ GPa} \pm 2\%$ ,  $D_0$  (outer diameter of the tube) =  $13.5 \text{ mm} \pm 0.10 \text{ mm}$ ,  $d_1 = 112.5 \pm 5 \text{ mm}$ , and  $H = 500 \pm 5 \text{ mm}$ , in the same direction, was determined and found to be 10.14%.

The calibration plots for the selected tube configurations have been illustrated in Fig. 3. The plots depict the variations in the actual mass flow rate measured against the corresponding time lag computed during the trials. It can be seen that the time lag measurement unit gives reasonably accurate results within the permissible limits. The data is found to be scattered within the range of  $[\pm 5 \text{ \%}]$  the best straight line fit.

The relationship between the Reynolds number (Re) and the error percentage for the Omega and Diamond tube geometries is depicted in Figure 4. It can be noted that the Omega tube configuration exhibits a reduced proportion of inaccuracy compared to the Diamond tube layout. Additionally, when the flow rate increases, the rate of

mistakes reduces. The distributed inaccuracy seen in the diamond tube arrangement relative to flow rate is highlighted in Figure 4. Vibrations of the supporting structure, manufacturing flaws in the tube shape (especially at bend parts), and the placement of the stinger—which should ideally be at the point of excitation—all may be responsible for the inaccuracy. Additionally, the plot demonstrates that the inaccuracy decreases with an increase in the flow rate.

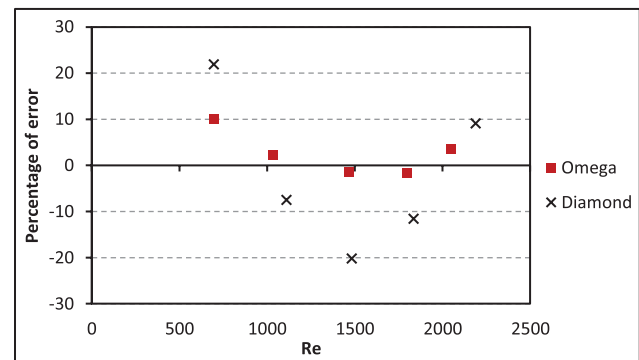
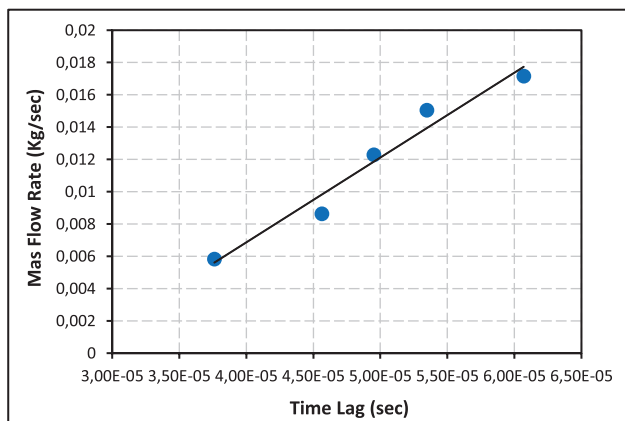


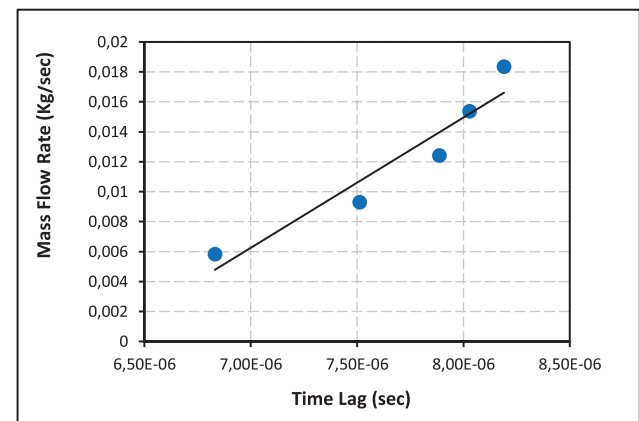
**Figure 4.** Percentage error variation for selected tube configuration.

**Model Development for CMFM and Implementation of Taguchi Approach**

The use of Design of Experiments (DOE) is a potent method to examine the connection between different elements influencing a process and its results. It is crucial to carry out tests methodically in order to collect data that can be used to analyse and support the phenomenon and understand its underlying physics. This objective can be accomplished in a number of ways, including the Taguchi



(a) Omega shape tube



(b) Diamond shape tube

**Figure 3.** Plot of mass flow rate versus time lag.

approach to experimental design and trial-and-error techniques. The Taguchi approach has been used in this study to create a mathematical model for comprehending the effect of design variables on the functionality of CMFM. Sensor position, excitation frequency, and flow range are the main considerations. In the Taguchi technique, an orthogonal array of experiments is utilised to measure variance and control it for optimum process parameters. An aim for optimisation is the Taguchi method’s signal-to-noise (S/N) ratio, which indicates the logarithm function of the predicted output. The S/N ratio, which represents the experimental results, shows how closely or how far a quality feature deviates from the ideal value. Table 3 presents the variables and parameters and their corresponding levels chosen for the experiments [14–15].

The Taguchi approach is a systematic procedure that includes several steps, such as identifying the characteristic to be optimised, choosing variables and their corresponding levels, choosing test conditions and noise factors, designing the experiment and layout, analysing the obtained data, determining the optimal levels of variables, and projecting the system’s performance at the optimal levels. As shown in Table 3, a L9 orthogonal array with nine experiments for three design elements and three levels was used in this work for each tube configuration. The experimental design matrix for all selected tube configurations is presented in Table 4.

The designed setup was used to carry out the experimental tests. Table 5 provides a summary of the time lag results from experimentation for several tube configurations and the accompanying parameter values.

**Table 3.** Experimental parameters and their levels

Tube configuration	Parameter	Level (1-Low, 2-Medium, 3-High)		
Omega shape	A-Sensor Position	A1 (1)	A2 (2)	A3 (3)
	B- Frequency (Hz)	B1 (52.74)	B2 (58.6)	B3 (64.46)
	C-Flow rate (kg/s)	C1 (0.008639694)	C2 (0.012296885)	C3 (0.015056554)
Diamond shape	A-Sensor Position	A1 (1)	A2 (2)	A3 (3)
	B- Frequency (Hz)	B1 (63.37)	B2 (70.41)	B3 (77.45)
	C-Flow rate (kg/s)	C1 (0.009047592)	C2 (0.01209065)	C3 (0.014970542)

**Table 4.** Experimental design matrix for selected tube configurations

Tube Shape	Expt. No.	Input		
		A	B	C
Omega Shape	1	1	1	1
	2	1	2	2
	3	1	3	3
	4	2	1	2
	5	2	2	3
	6	2	3	1
	7	3	1	3
	8	3	2	1
	9	3	3	2
Diamond Shape	1	1	1	1
	2	1	2	2
	3	1	3	3
	4	2	1	2
	5	2	2	3
	6	2	3	1
	7	3	1	3
	8	3	2	1
	9	3	3	2

**Table 5.** Levels of parameters and experimental values of time lag for selected tube configurations

Tube Configuration	Expt. No.	Sensor Position (A) mm	Frequency of Vibration (B) Hz	Flow Rate (C) kg/s	Time Lag sec
Omega Shape	1	1	52.74	0.008639694	2.493707E-05
	2	1	58.6	0.012296885	4.352394E-05
	3	1	64.46	0.015056554	3.451108E-05
	4	2	52.74	0.012296885	3.880309E-05
	5	2	58.6	0.015056554	5.347030E-05
	6	2	64.46	0.008639694	3.291296E-05
	7	3	52.74	0.015056554	3.902273E-05
	8	3	58.6	0.008639694	3.8905849E-05
	9	3	64.46	0.012296885	3.5708816E-05
Diamond Shape	1	1	63.37	0.009047592	2.98982E-06
	2	1	70.41	0.01209065	4.65116E-06
	3	1	77.45	0.014970542	3.98254E-06
	4	2	63.37	0.01209065	3.09039E-06
	5	2	70.41	0.014970542	8.02833E-06
	6	2	77.45	0.009047592	4.84161E-06
	7	3	63.37	0.014970542	8.86538E-06
	8	3	70.41	0.009047592	1.21381E-05
	9	3	77.45	0.01209065	1.32121E-05

Sensor Position Notation: 1-SP1, 2-SP2, 3-SP3

## RESULTS AND DISCUSSION

### Analysis of Variance

Using the mathematical software programme MINITAB 17, the experiment's outcomes were examined. The time lag data was analysed using an ANOVA, and various plots for regression and graphical analysis were made. It was found that the three variables—sensor position (A), vibration frequency (B), and mass flow rate—together make up the linear response function for the time lag (C). In order to determine how these parameters affected the outcome, an analysis of variance was used. The best-suited model was chosen based on a Prob > F value of less than 0.05. Due to its low standard deviation and high R2 values, it was determined through the analysis of experimental data that the quadratic model fit the Omega tube layout the best. The quadratic model perfectly suited the experimental data, as shown by the R2 value of 0.9964. The linear model, on the other hand, was found to suit the diamond-shaped tube design the best, with an R2 value of 0.7798, suggesting a nearly perfect fit. Since the projected values of the time lag nearly matched the observed values, the regression model was deemed to be a satisfactory fit for the experimental

data [16]. Minitab 17 was used to create the interaction and main effect charts for each tube arrangement.

### A. Omega shape tube configuration

The time lag experimental results and anticipated values for the Omega tube configuration from the regression model are compared in Figure 5. The graphic demonstrates how closely the projected values match the experimental values, demonstrating how well the regression model fits the experimental data. Results from the experiment are shown in Table 6's ANOVA table.

The interaction effect of variables on the time lag is depicted in Figure 6. The graphic shows how the relationship between two variables influences the time lag. These graphical representations show the relationship between the design variables and their effects on the time lag. The figure enables us to see how the interplay of the variables affects the time lag. The major effect plot, shown in Figure 7, illustrates how the chosen parameters affect the time lag. While the other variables are held constant, the plot displays the specific impact of each variable on the time lag. The figure makes it crystal clear how the chosen settings affect the CMFM's time lag. When vibrated at the tube's

Table 6. Analysis of variance

Source	DF	Contribution (%)	F value	P Value	Parameter Significance
Regression	6	99.64	91.45	0.011	
Sensor Position (A)	1	3.90	28.39	0.012	Insignificant
Frequency of vibration (B)	1	0.00	73.17	0.004	Insignificant
Mass flow rate (C)	1	30.08	28.39	0.033	Significant
Error	2	0.36			
Total	8	100.00			

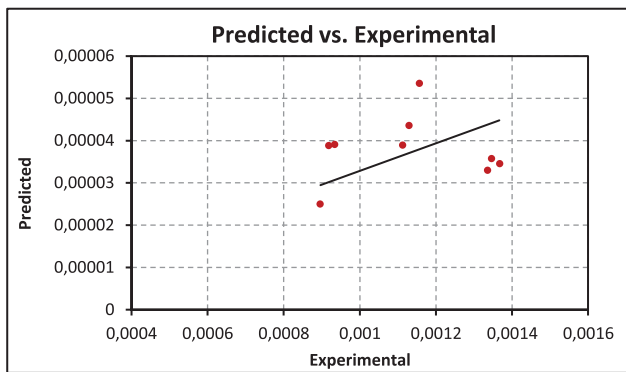


Figure 5. Plot of the predicted vs. experimental values of time lag for Omega shape tube.

natural frequency, the Omega-shaped tube configuration has been found to function best among the two configurations being studied, with the sensor position set along the tube’s centre line. The flow rate, however, has been the factor that has had the most impact on the meter output, as seen by the interaction and main effect plots. As a result, the flow rate that is anticipated has a major impact on the meter output of an Omega tube arrangement. The constant curvature of the Omega tube configuration reduces secondary flow while providing the least amount of resistance to flow disruption. This will cause the Coriolis effect to be as strong as possible, increasing tube twist and creating the longest time lag in the laminar area.

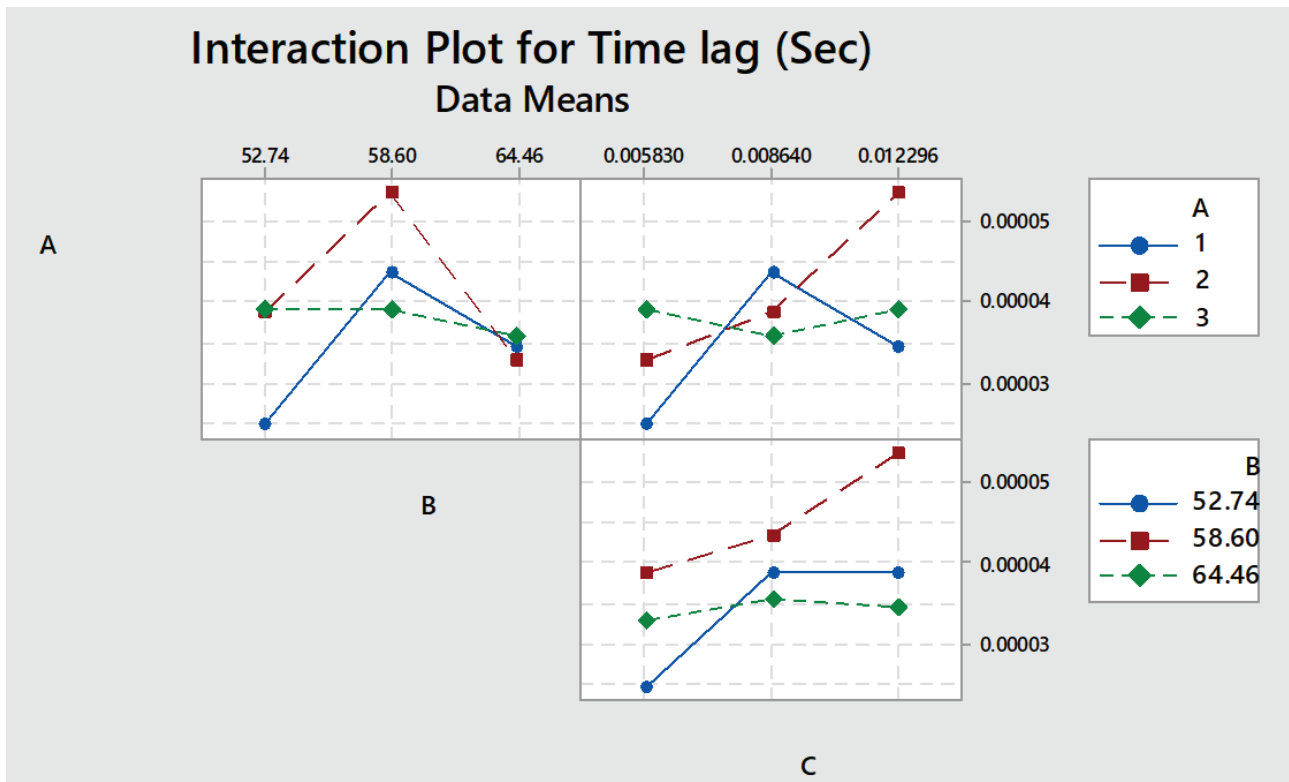


Figure 6. Interaction plot of time lag for Omega shape tube.

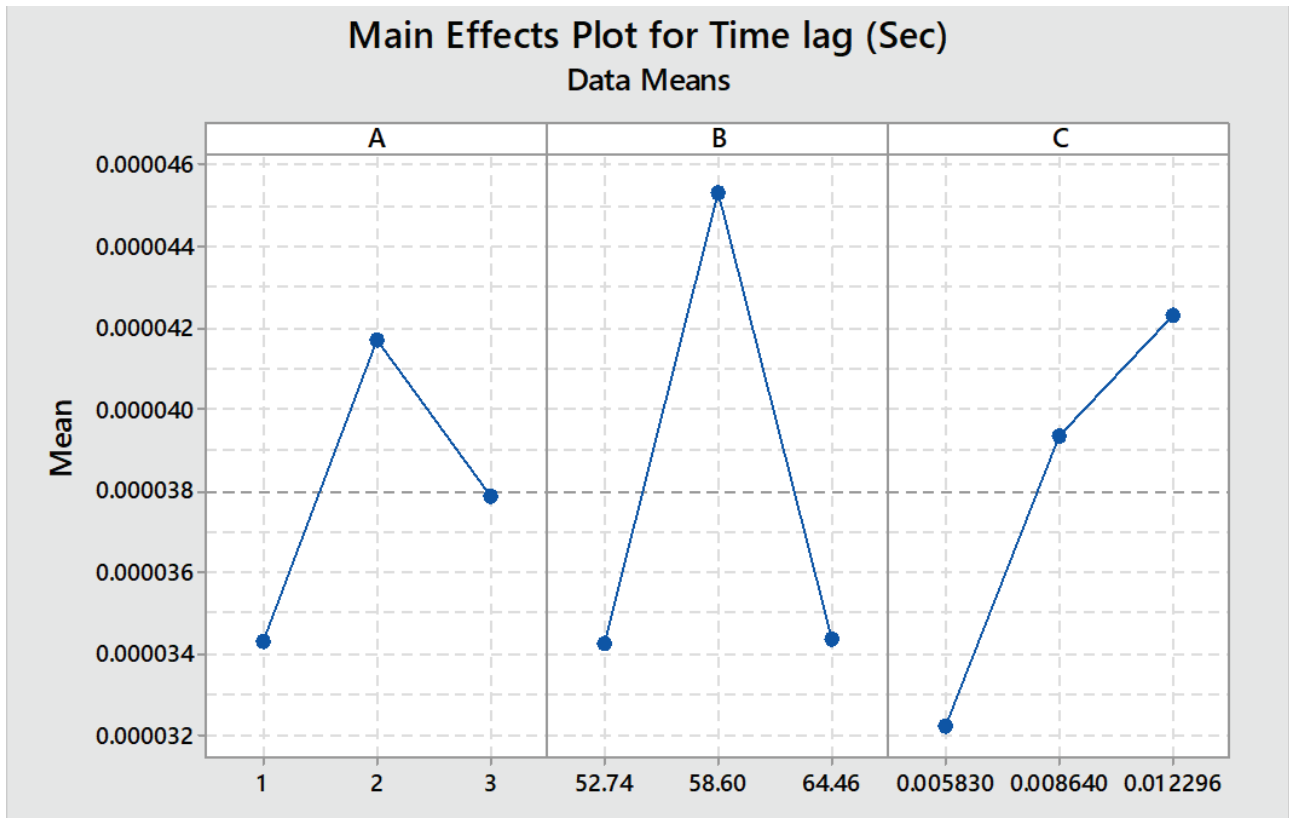


Figure 7. Main effect plot of time lag for Omega shape tube.

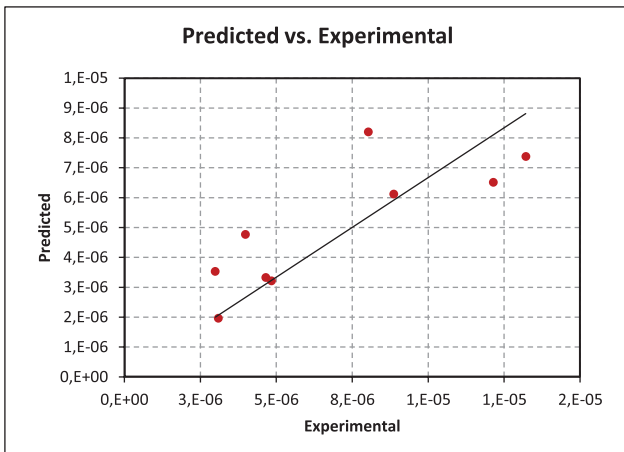
**B. Diamond shape tube configuration**

Figure 8 shows a comparison of the experimental and expected values of the time lag for a diamond tube design. Additionally, Figures 9 and 10 show, respectively, the interaction plot and the main effect plot of the factors for time lag. The relationship between the design variables and their impact on the time lag is revealed by these graphical depictions. The examination of these plots enables the determination of the design variables' optimum values for obtaining the intended system performance. It has been established that the regression model

created for the diamond tube arrangement is adequate since it produces good agreement between the anticipated and experimental time lag values. This indicates that the selected design variables and their corresponding levels have a significant impact on the performance of the system. The most determining factor has been identified as the sensor position, and changing the sensor placement has a significant impact on the meter output. The meter's response time to changes in flow rate and tube vibration frequency was found to be slow, which limited the laminar region's applicability. Due to the complex shape of the

Table 7. Analysis of variance

Source	DF	Contribution %	F-value	P-value	Parameter Significance
Regression	3	77.98	5.9	0.043	
Sensor Position (A)	1	70.88	16.09	0.010	Significant
Frequency of vibration (B)	1	6.98	1.59	0.264	Insignificant
Mass flow rate (C)	1	0.12	0.03	0.877	Insignificant
Error	5	22.02			
Total	8	100.00			



**Figure 8.** Plot of the predicted vs. experimental values of time lag for Diamond shape tube.

diamond tube configuration, the flowing fluid continuously experiences disturbance while flowing through successive straight portions of the configuration. This boosts the secondary flow, lessening the Coriolis effect and the corresponding tube twist. It has been discovered that sensor position—rather than flow rate—is the determining factor in the meter’s output.

**Inferences of Interaction Plot**

Each tube configuration’s interaction and main effect plots were carefully studied, and the results are reported in Table 8. The table displays the degrees of interaction between the best individual parameters for maximising the outcome and the interaction parameters.

**Analysis of Signal-to-Noise (S/N) Ratio**

The signal-to-noise (S/N) ratio is a commonly used metric in engineering applications for predicting the deviation of quality characteristics from desired values. It represents the ratio of the expected signal (the desired outcome value) to noise (the undesired value, which is the squared deviation of the output characteristics). The S/N ratio is typically calculated as the log function of the desired output or the inverse of variance and serves as the objective function of optimisation. Analysing data using this ratio can predict the optimum output, where the maximum S/N ratio indicates the minimum variability of the process against the undesirable changes in noise factors. The selected factors or parameters should yield the maximum S/N ratio to maintain minimum variability. In different cases, the optimum S/N ratio can be lower, higher, or nominal. In this study, a higher time lag value is desired, and hence, the S/N ratio is maintained higher using MINITAB 17. Each factor level combination’s signal-to-noise (S/N) ratio is determined.

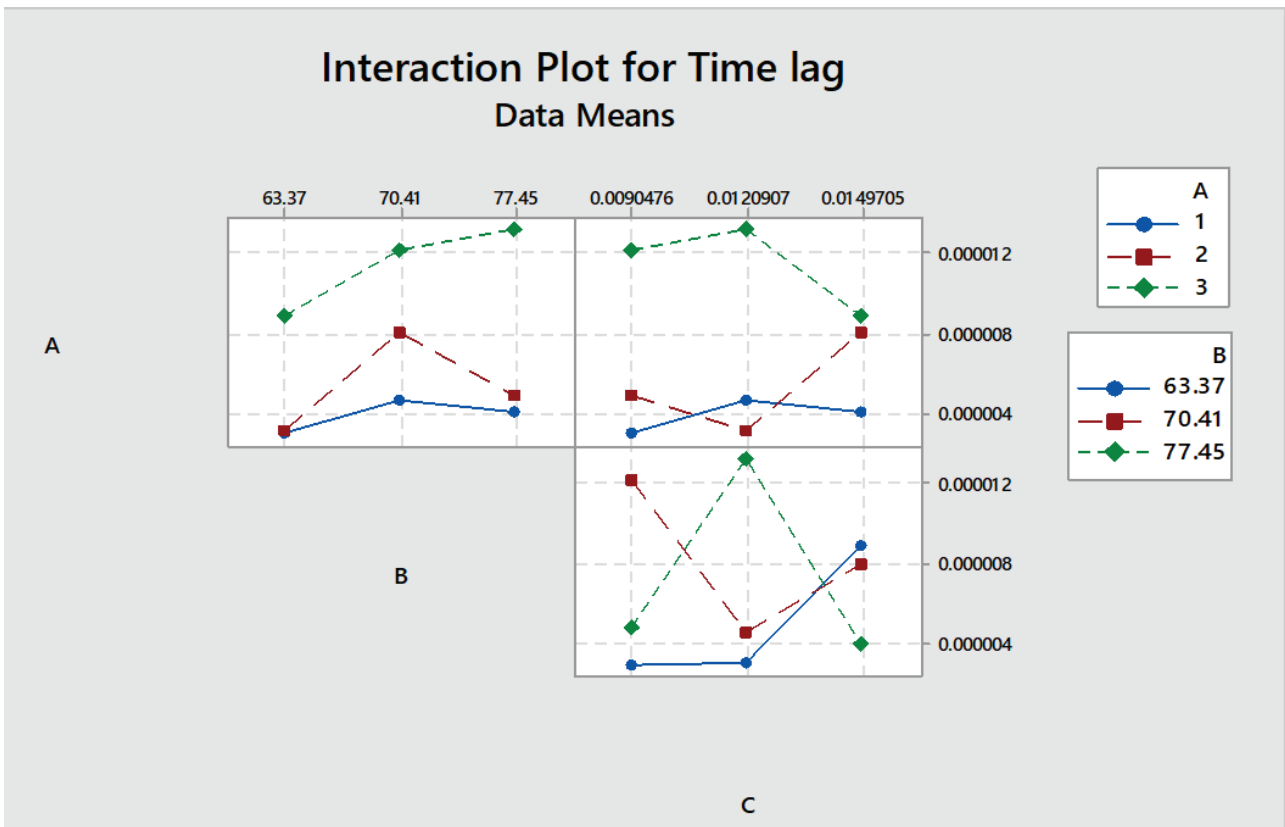


**Figure 9.** Interaction plot of time lag for Diamond shape tube.

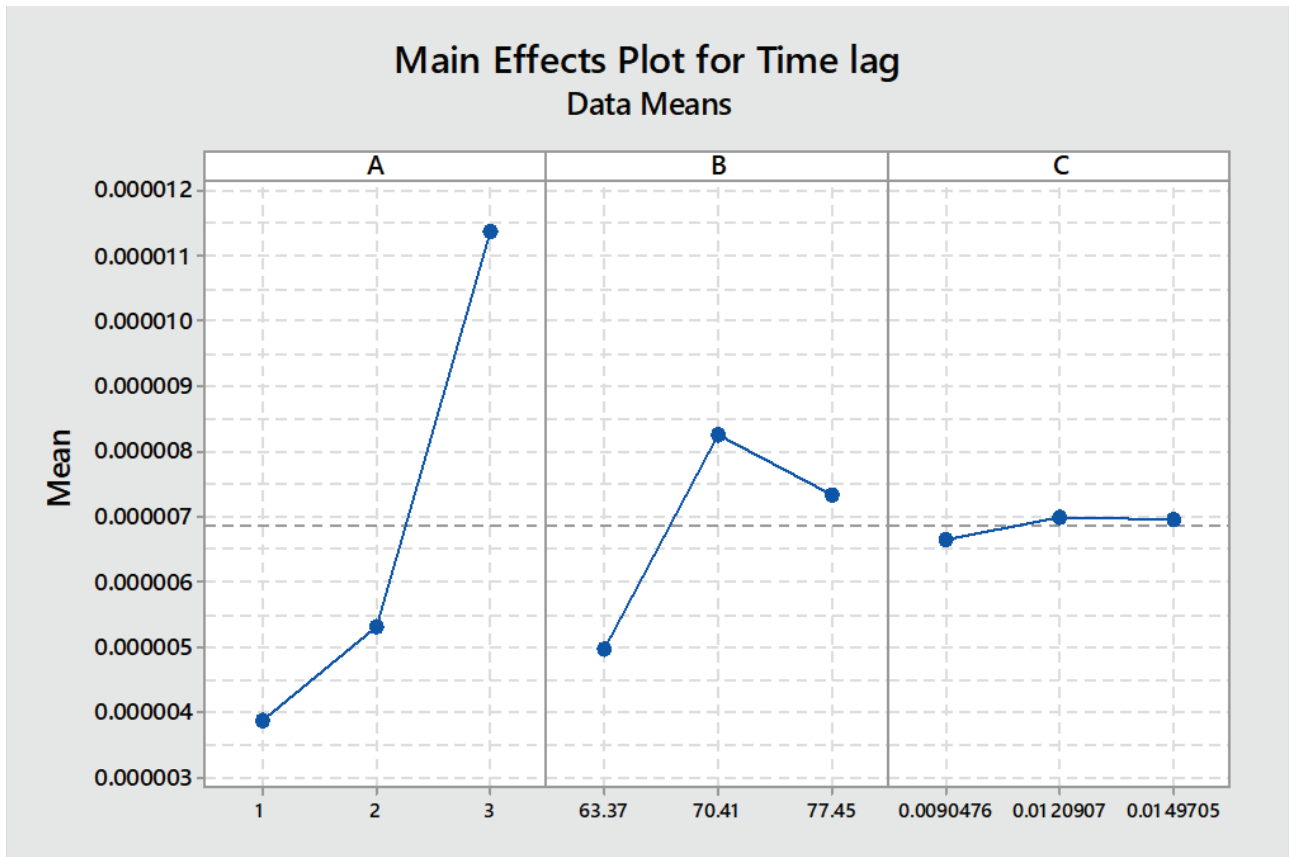


Figure 10. Main effect plot of time lag for Diamond shape tube.

The larger-is-better S/N ratio using base 10 log is calculated as follows [16]:

$$\left(\frac{S}{N}\right)_{LB} = -10 \log \left( \frac{\left( \frac{1}{y^2_1} + \frac{1}{y^2_2} + \frac{1}{y^2_3} + \dots + \frac{1}{y^2_n} \right)}{n} \right) \quad (5)$$

where n is the total number of experiments and Y is the experimental results/observations.

Table 9 summarises the signal-to-noise ratio (S/N ratio) for selected tube configurations (Omega and Diamond) for three different parameters: sensor location,

frequency of tube vibration, and flow rate (A-sensor position, B-frequency of tube vibration, and C-flow rate). A larger-is-better S/N ratio in this situation denotes a more precise and trustworthy measurement. The value that is highlighted in the table denotes the level and parameter values that correspond to a higher S/N ratio and an optimal time lag reading from the meter. For instance, in the case of an Omega tube arrangement, a higher S/N ratio is associated with a certain combination of characteristics, including sensor position (SP2), tube vibration frequency (F2), and flow rate (FR3). The largest time lag is produced by this combination of factors.

Table 8. Summary of the interaction plot and individual best parameters for the selected tube configurations

Tube Configuration	Plot	Interaction Parameters	Level of Interaction	Individual Best Parameters
Omega	6A	A and B	High	SP2, F2, FR3
	6B	A and C	High	
	6C	B and C	Medium	
Diamond	10A	A and B	Low	SP3, F2, FR2
	10B	A and C	Medium	
	10C	B and C	High	

Table 9. S/N ratio for the selected tube configurations

Tube Shape	Expt. No.	Input			Output	S/N Ratio		
		A	B	C	Time lag ( $\mu$ s)			
Omega Shape	1	1	52.74	0.008639694	24.93707	621.86	2.79	-27.94
	2	1	58.6	0.012296885	43.52394	1894.33	3.28	-32.77
	3	1	64.46	0.015056554	34.51108	1191.01	3.08	-30.76
	4	2	52.74	0.012296885	38.80309	1505.68	3.18	-31.78
	5	2	<b>58.6</b>	<b>0.015056554</b>	<b>53.47030</b>	<b>2859.07</b>	<b>3.46</b>	<b>-34.56</b>
	6	2	64.46	0.008639694	32.91296	1083.26	3.03	-30.35
	7	3	52.74	0.015056554	39.02273	1522.77	3.18	-31.83
	8	3	58.6	0.008639694	38.905849	1513.67	3.18	-31.80
	9	3	64.46	0.012296885	35.708816	1275.12	3.11	-31.06
Diamond Shape	1	1	63.37	0.009047592	2.989822	8.94	0.95	-9.51
	2	1	70.41	0.01209065	4.65116	21.63	1.34	-13.35
	3	1	77.45	0.014970542	3.98254	15.86	1.20	-12.00
	4	2	63.37	0.01209065	3.090386	9.55	0.98	-9.80
	5	2	70.41	0.014970542	8.02833	64.45	1.81	-18.09
	6	2	77.45	0.009047592	4.841614	23.44	1.37	-13.70
	7	3	63.37	0.014970542	8.86538	78.59	1.90	-18.95
	8	3	70.41	0.009047592	12.138139	147.33	2.17	-21.68
	9	3	<b>77.45</b>	<b>0.01209065</b>	<b>13.21216</b>	<b>152.81</b>	<b>2.18</b>	<b>-21.84</b>

## CONCLUSION

The Design of Experiments (DOE) by Taguchi method is a powerful statistical tool used to analyze experimental data and predict the impact of design parameters on time lag results. In this study, mathematical model equations were derived using MINITAB 17, which are either quadratic or linear, representing the time lag, and expressed as a function of design parameters. This enables researchers to gain valuable insights into the relationships between the design parameters and the time lag, allowing for more efficient and effective optimization of the system. Some of the salient observations of DOE by the Taguchi approach and ANOVA are:

The predicted time lag values obtained from the mathematical model equations derived by using MINITAB 17 were found to be in good agreement with the experimental values.

- It was noted that the predicted time lag values and the experimental findings showed a good degree of agreement.
- The Omega tube design's interaction plot showed strong interactions between the parameters and time lag, with all of the lines interacting with one another.

- For the Omega tube design, the largest time lags were observed at sensor position SP2, frequency F2, and flow rate FR3.
- The diamond tube structure, in comparison, showed a modest amount of parameter and time lag interaction.
- The flow rate and sensor position were found to be the most crucial variables for the Omega tube and diamond tube arrangements, respectively.
- The sensor position SP3, frequency F2, and flow rate FR2 were found to be the best set of characteristics for the diamond tube layout. Different factors affected the time lag in different ways, depending on how the tubes were arranged. Omega tube configuration was shown to be primarily influenced by flow rate (30.08%), whereas Diamond tube configuration was primarily influenced by sensor position (70.88%).
- It has been observed that different factors have varying effects on time lag, depending on the configuration of the tube.
- The experiment's and ANOVA's findings show that time lag is a function of sensor position, vibration frequency, and mass flow rate, and that the ideal set of parameters for the best outcomes differs depending on the tube configuration.

## NOMENCLATURE

$\dot{m}$	Mass flow rate (kg/s)
$K_s$	Torsional stiffness of the tube ( Nm/rad)
$\Delta t$	Time lag (s)
$d_1$	Semi-distance between the two arms of the tube (m)
$E$	Modulus of elasticity of the tube material (GPa)
$I$	Moment of inertia of the tube cross section (m <sup>4</sup> )
$H$	Length of the tube (m)
$n_1$	H/ $d_1$ ratio
$C$	Flow correction factor
$K$	Poisson's ratio

## AUTHORSHIP CONTRIBUTIONS

Authors equally contributed to this work.

## DATA AVAILABILITY STATEMENT

The authors confirm that the data that supports the findings of this study are available within the article. Raw data that support the finding of this study are available from the corresponding author, upon reasonable request.

## CONFLICT OF INTEREST

The author declared no potential conflicts of interest with respect to the research, authorship, and/or publication of this article.

## ETHICS

There are no ethical issues with the publication of this manuscript.

## REFERENCES

- [1] Kumar V, Anklin M. Numerical Simulations of Coriolis Flow Meters for Low Reynolds Number. *Flows J Metrol Soc India* 2011;26:225–235. [\[CrossRef\]](#)
- [2] Gupta P, Srinivasan K, Prabhu S. Tests on various configurations of Coriolis mass flowmeters. *Measurement* 2006;39:296–307. [\[CrossRef\]](#)
- [3] Sharma S, Patil P, Vasudev A, Jain S. Performance evaluation of an indigenously designed copper (U) tube Coriolis mass flow sensors. *Measurement* 2010;43:1165–1172. [\[CrossRef\]](#)
- [4] Patil P, Sharma S, Jain S. Response surface modeling of vibrating omega tube (Copper) electromechanical Coriolis mass flow sensor. *Expert Syst Appl* 2012;39:4418–4426. [\[CrossRef\]](#)
- [5] Patil P, Sharma S, Jain S. Performance evaluation of a copper omega type Coriolis mass flow sensor with an aid of ANFIS tool. *Expert Syst Appl* 2012;39:5019–5024. [\[CrossRef\]](#)
- [6] Patil P, Sharma S, Jain S. Prediction modeling of coriolis type mass flow sensor using neural network. *Instrum Exp Tech* 2011;54:435–439. [\[CrossRef\]](#)
- [7] Patil P, Sharma S, Paliwal V, Kumar A. ANN modelling of Cu type omega vibration based mass flow sensor. *Proced Technol* 2014;14:260–265. [\[CrossRef\]](#)
- [8] Patil P, Sharma S, Jaiswal H, Kumar A. Modeling influence of tube material on vibration based EMMFs using ANFIS. *Procedia Mater Sci* 2014;6:1097–1103. [\[CrossRef\]](#)
- [9] Kolhe V, Edlabadkar R. Performance evaluation of Coriolis mass flow meter in laminar flow regime. *Flow Meas Instrum* 2021;77:1–13. [\[CrossRef\]](#)
- [10] Sharma S, Bhattacharya M, Khaliqzama M, Sapra A. Development of a mass flow rate meter based on Coriolis effect. *Int J Mech Eng Educ* 2015;29:132–146. [\[CrossRef\]](#)
- [11] Baker R. Coriolis flowmeters: Industrial practice and published information. *Flow Meas Instrum* 1994;5:229–246. [\[CrossRef\]](#)
- [12] Baker R. *Flow Measurement Handbook*. Cambridge: Cambridge University Press; 2000.
- [13] Pei X, Li X, Xu H, Zhang X. Flow-induced vibration characteristics of the U-type Coriolis mass flowmeter with liquid hydrogen. *J Zhejiang Univ Sci A* 2022;23:495–504. [\[CrossRef\]](#)
- [14] Ghalme S, Mankar A, Bhalerao Y. Parameter optimization in milling of glass fiber reinforced plastic (GFRP) using DOE-Taguchi method. *Springer Plus* 2016;5:1376. [\[CrossRef\]](#)
- [15] Ghalme S, Mankar A, Bhalerao Y. Optimization of wear loss in silicon nitride (Si<sub>3</sub>N<sub>4</sub>)-hexagonal boron nitride (hBN) composite using DoE-Taguchi method. *Springer plus*. 2016;5:1671. [\[CrossRef\]](#)
- [16] Ghalme S, Mankar A, Bhalerao Y. Original Integrated Taguchi-simulated annealing (SA) approach for analyzing wear behaviour of silicon nitride. *J Appl Res Technol* 2018;15:624–632. [\[CrossRef\]](#)
- [17] Khan M, Nadeem S. Theoretical treatment of bio-convective Maxwell nanofluid over an exponentially stretching sheet. *Can J Phys* 2019;98:732–741. [\[CrossRef\]](#)
- [18] Nadeem S, Khan M, Muhammad N, Ahmad S. Mathematical analysis of bio-convective micropolar nanofluid. *J Comput Des Eng* 2019;6:233–242. [\[CrossRef\]](#)
- [19] Khan M, Nadeem S, Muhammad N. Micropolar fluid flow with temperature-dependent transport properties. *Heat Transf* 2020;49:2375–2389. [\[CrossRef\]](#)
- [20] Ahmad S, Nadeem S, Muhammad N, Khan M. Cattaneo-Christov heat flux model for stagnation point flow of micropolar nanofluid toward a nonlinear stretching surface with slip effects. *J Therm Anal Calorim* 2021;143:1187–1199. [\[CrossRef\]](#)
- [21] Ahmad S, Khan M, Nadeem S. Mathematical analysis of heat and mass transfer in a Maxwell fluid with double stratification. *Phys Scr* 2020;96:025202. [\[CrossRef\]](#)

- [22] Khan M, Ullah N, Nadeem S. Transient flow of Maxwell nanofluid over a shrinking surface: Numerical solutions and stability analysis. *Surf Interfaces* 2021;22:100829. [\[CrossRef\]](#)
- [23] Khan M, Nadeem S, Saleem A. Mathematical analysis of heat and mass transfer in a Maxwell Fluid. *Proc Inst Mech Eng C J Mech Eng Sci* 2020;235:4967–4976. [\[CrossRef\]](#)
- [24] Khan M, Nadeem S. A comparative study between linear and exponential stretching sheet with double stratification of a rotating Maxwell nanofluid flow. *Surf Interf* 2021;22:100886. [\[CrossRef\]](#)
- [25] Nadeem S, Khan M, Nadeem A. Transportation of slip effects on nanomaterial micropolar fluid flow over exponentially stretching. *Alex Eng J* 2020;59:3443–3450. [\[CrossRef\]](#)
- [26] Haider J, Muhammad N. Computation of thermal energy in a rectangular cavity with a heated top wall. *Int J Mod Phys B* 2022;36:2250212. [\[CrossRef\]](#)
- [27] Haider J, Ahammad N, Khan M, Guedri K, Galal A. Insight into the study of natural convection heat transfer mechanisms in a square cavity via finite volume method. *Int J Mod Phys B* 2022;37:2350038. [\[CrossRef\]](#)
- [28] Raza M, Haider J, Ahammad N, Guedri K, Galal A. Insightful study of the characterization of the Cobalt oxide nanomaterials and hydrothermal synthesis. *Int J Mod Phys B* 2022;37:2350101. [\[CrossRef\]](#)
- [29] Nadeem S, Haider J, Akhtar S, Ali S. Numerical simulations of convective heat transfer of a viscous fluid inside a rectangular cavity with heated rotating obstacles. *Int J Mod Phys B* 2022;36:2250200. [\[CrossRef\]](#)
- [30] Asghar S, Haider J, Muhammad N. The modified KdV equation for a nonlinear evolution problem with perturbation technique. *Int J Mod Phys B* 2022;36:2250160. [\[CrossRef\]](#)
- [31] Haider J, Ahmad S. Dynamics of the Rabinowitsch fluid in a reduced form of elliptic duct using finite volume method. *Int J Mod Phys B* 2022;36:2250217. [\[CrossRef\]](#)
- [32] Rahman J, Mannan A, Ghoneim M, Yassen M, Haider, J. Insight into the study of some nonlinear evolution problems: Applications based on Variation Iteration Method with Laplace. *Int J Mod Phys B* 2022;37:2350030. [\[CrossRef\]](#)
- [33] Haider J, Muhammad N. Mathematical analysis of flow passing through a rectangular nozzle. *Int J Mod Phys B* 2022;36:2250176. [\[CrossRef\]](#)
- [34] Zahid M, Younus A, Ghoneim M, Yassen M, Haider J. Quaternion-valued exponential matrices and its fundamental properties. *Int J Mod Phys B* 2022;37:2350027. [\[CrossRef\]](#)
- [35] Haider J, Asghar S, Nadeem S. Travelling wave solutions of the third-order KdV equation using Jacobi elliptic function method. *Int J Mod Phys B* 2022;37:2350117. [\[CrossRef\]](#)